THE JOURNAL OF PHYSICAL CHEMISTRY B

Article

pubs.acs.org/JPCB

Statics and Dynamics of Free and Hydrogen-Bonded OH Groups at the Air/Water Interface

Ana Vila Verde,*[,†,§] Peter G. Bolhuis,*[,†] and R. Kramer Campen*[,‡]

[†]Van't Hoff Institute for Molecular Science, University of Amsterdam, P.O. Box 94157, 1090 GD Amsterdam, The Netherlands

[‡]Fritz Haber Institute of the Max Planck Society, Faradayweg 4-6, 14195 Berlin, Germany

Supporting Information

ABSTRACT: We use classical atomistic molecular dynamics simulations of two water models (SPC/E and TIP4P/2005) to investigate the orientation and reorientation dynamics of two subpopulations of OH groups belonging to water molecules at the air/water interface at 300 K: those OH groups that donate a hydrogen bond (called "bonded") and those that do not (called "free"). Free interfacial OH groups reorient in two distinct regimes: a fast regime from 0 to 1 ps and a slow regime thereafter. Qualitatively similar behavior was reported by others for free OH groups near extended hydrophobic surfaces. In contrast, the net reorientation of bonded OH groups occurs at a rate similar to that of bulk water. This similarity in reorientation rate results from compensation of two effects: decreasing frequency of hydrogen-bond breaking/formation (i.e., hydrogen-bond exchange) and faster rotation of intact hydrogen bonds. Both changes result from the decrease in density at the air/water interface relative to the bulk. Interestingly, because of the presence of capillary waves, the slowdown of hydrogen-bond exchange is significantly smaller than that reported for water near extended hydrophobic surfaces, but it is almost identical to that reported for water near small hydrophobic solutes. In this sense water at the air/water interface has characteristics of water of hydration of both small and extended hydrophobic solutes.

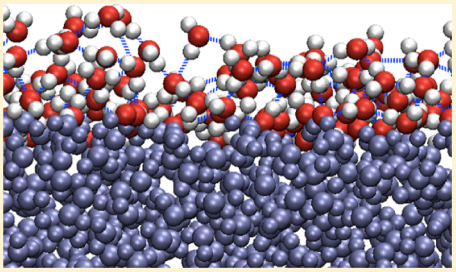

1. INTRODUCTION

The chemistry and physics of water at interfaces control a variety of important processes in the atmosphere, in biology, and in devices. Predictive understanding of these processes generally requires knowledge of their molecular level mechanisms. In particular, we often require an understanding of the relationship between the angstrom scale static and dynamic properties of water (at interfaces) and macroscopic thermodynamic observables. For example, accurate description of the free energy of adsorption of metal ions at the oxide−water interface requires knowledge of the dielectric constant of interfacial water and, thus, of interfacial water structure.[1,2] Experimental advances in the past 20 years have revolutionized our ability to quantify equilibrium properties as well as subpicosecond structural dynamics of water both in the bulk and around small solutes.[3−7] Contemporaneous advances in computational power and algorithms have enabled the calculation of experimental observables with water models of increasing complexity: fixed charge classical atomistic models, classical polarizable models, and ab initio molecular dynamics. Gaining similar insight into dynamics at extended interfaces has been challenging. At the experimental level this challenge arises because most techniques applied to the structural dynamics of neat water and water containing small solutes—IR absorbance, NMR, and dielectric relaxation—are not interface specific; thus their use to study interfacial water generally requires special sample cells to diminish the much larger signal from water molecules in the bulk. For vibrational spectroscopy this limitation can be overcome by application of the interface-specific, laser-based technique vibrational sum frequency (VSF) spectroscopy.[8] In the computational realm, calculation of interfacial water properties requires significantly larger system sizes and larger sampling times (e.g., simulations must be of sufficient length that small solutes reach an equilibrium between the bulk and the interface) than those in the bulk. It is thus only recently that widespread application of ab initio molecular dynamics approaches to simple aqueous interfaces has occurred.[9,10]

Above we have made the case for the importance of understanding the structure and structural dynamics of interfacial water in general. In this study we address in particular the structure and structural dynamics of water at the air/water interface. We choose to focus in this manner for three reasons: several studies have found that water at the air/water interface is strikingly similar to water near hydrophobic interfaces more generally;[8,10,11] properties of the air/water interface control a variety of chemical processes in the atmosphere and in the surface ocean;[12] from an experimental perspective its study is easier than that of other water/hydrophobic interfaces.

Following the pioneering VSF spectroscopy work of Shen and co-workers, a variety of computational and experimental

Received: April 30, 2012
Revised: July 10, 2012
Published: July 12, 2012

dx.doi.org/10.1021/jp304151e | J. Phys. Chem. B 2012, 116, 9467−9481

studies have determined that, on average, there are two types of water at the air/water interface.[10,13−17] The first type straddles the interface with one non-hydrogen-bonded OH pointing toward the vapor and the other hydrogen-bonded OH pointing into the bulk. The second donates two hydrogen bonds, both of which point approximately toward the bulk. Both computational approaches and VSF studies suggest that ≈25% of OH groups at the interface point toward the vapor and are not hydrogen-bonded. While the average structure of the air/water interface has thus been considerably clarified, its structural dynamics are much less well understood. Several questions are of interest: Do the two types of water at the air/water interface rotate or translate at different rates or by different mechanisms? Do either their rotation/translation rates or mechanisms differ from those of water in the bulk? As noted above, it is difficult to answer these questions in experiment, as the methods most often employed to study water structural dynamics in the bulk cannot straightforwardly be used to study the dynamics of water at the air/water interface. Such hurdles do not exist in simulation, and there have been a variety of studies that describe rotation and translation of interfacial water using water models of varying complexity.[9,18−20] Far fewer studies have focused on the dynamics and mechanism of hydrogen-bond breaking and re-formation and their relationship to structural dynamics in this environment (our previous combined experimental and computational study is an exception to this trend[8]).

Over the past few years the rotation of water in the bulk and around small solutes on subpicosecond time scales has been shown, principally through computational studies by Hynes, Laage, and co-workers, to be nondiffusive: water in these environments rotates via infrequent large-amplitude angular jumps, each of which accompanies the breaking of an existing hydrogen bond and the formation of a new one involving a new acceptor.[21,22] In several recent papers the same group has demonstrated that water at idealized, solid hydrophobic and hydrophilic interfaces appears to also rotate nondiffusively and, with the notable exception of one class of OH groups at an idealized hydrophobic interface, to be slowed relative to rotation in the bulk.[23,24] Recently we and others published a combined polarization resolved, IR pump−vibrational sum frequency probe, computational study of the structural dynamics of free OH groups at the air/water interface.[8] In that study we demonstrated that free OH groups at the air/water interface rotate ≈3 times faster than bulk water and do so diffusively.[8] That study is notable both because it is the first experimental quantification of water rotational dynamics at extended interfaces that is both label-free and considers the nonlinear optical response, and because the agreement between simulation and experiment obtained without adjustable parameters lends confidence in our ability to rationalize the experimentally observed structural dynamics in terms of hydrogen-bond breaking and re-formation as well as structural evolution apparent in the simulation.

In our previous study we focused solely on free OH groups because of limitations on probing interfacial hydrogen-bonded OH groups in pure H_2O arising from ultrafast nonradiative energy transfer. Such limitations are absent from simulation, so here we report an in-depth computational study of the structure and dynamics of interfacial OH groups and evaluate differences between free and hydrogen-bonded ones. Two well-known classical water models (SPC/E and TIP4P/2005[25−28]) are used here, and they lead to similar results. We find that hydrogen-bonded OH groups at the air/water interface, in contrast to free OH groups, rotate at rates similar to those of OH groups in bulk water and do so by a similar nondiffusive jump mechanism. Interestingly, this similar reorientation rate to bulk water is the result of two competing effects that largely counteract each other: large-amplitude angular jumps (the breaking and formation of new hydrogen bonds) are less frequent than in bulk water (slowing rotation), while the rotation of intact hydrogen bonds between jumps is more rapid. Both effects can be understood by accounting for the reduced average density of water near the air/water interface relative to the bulk.

The remainder of this paper is organized as follows. In section 2 we describe the computational methods employed. To understand the ultrafast structural and hydrogen-bond dynamics of OH groups at the interface, we require a quantitative interfacial definition. To build this foundation, we discuss in section 3 the time-averaged density profile and OH orientation at the air/water interface as a function of water coordination. In section 4 we consider the rotational dynamics of interfacial water, then discuss the hydrogen-bond dynamics of the hydrogen-bonded OH and how they differ from those of free OH, and rationalize the observed changes in rotational and hydrogen-bond dynamics through extension of the *extended jump model* previously described by Laage and Hynes.[21]

2. METHODS

We performed all-atom molecular dynamics simulations, of SPC/E and TIP4P/2005 water slabs and water in the bulk, using the molecular dynamics package NAMD.[25−29] The two water models are both fixed charge, classical all-atom descriptions but differ in the location of charge on the water molecule. Studying both allows us to conclude, as shown in detail below, that our results are essentially insensitive to this parameter at the simulated temperature (300 K). The package VMD (Visual Molecular Dynamics) was used for trajectory visualization and analysis.[30] Electrostatic interactions were calculated directly up to 15 Å and using the particle mesh Ewald method with 1 Å grid spacing at larger separation. The van der Waals (vdW) interactions were smoothly switched to zero between 13 and 15 Å, and long-range corrections were not applied. The unusually large cutoff for vdW interactions was chosen because the long-range contribution of these interactions is, in general, necessary for better agreement of interfacial properties such as the surface tension with experiment.[31−33] Such long vdW cutoffs are required even for systems—such as the air/water interface—where electrostatic interactions dominate.[34,35] A modified Verlet algorithm with multiple time stepping was used for integration, with bonded and vdW forces calculated every 1 fs, and electrostatic forces calculated every 10 fs. The SHAKE algorithm was used to fix all bond lengths. The initial water slabs containing 826 water molecules were created using the water box plug-in in VMD. Both TIP4P/2005 and SPC/E systems were equilibrated for 1 ns in the canonical ensemble at 300 K. This procedure ensures the formation of a stable water slab, shown in Figure 1. Production runs, one for each water model, were performed in the microcanonical ensemble for 0.4 ns, with configurations saved every 2 fs. Periodic boundary conditions were used. The average temperatures during the production runs were $T_{SPC/E} = T_{TIP4P/2005} = 300 \pm 5$ K. The total energy drift was $<6 \times 10^{-3}$%. Unless otherwise indicated, the statistical uncertainty of

dx.doi.org/10.1021/jp304151e | J. Phys. Chem. B 2012, 116, 9467−9481

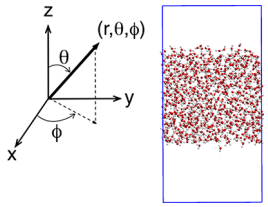

Figure 1. Geometry of the simulated water slab and coordinate system used during analysis. The center of mass is at $z = 0$. The box dimensions are $30 \times 30 \times 60$ Å^3.

reported quantities is given as the standard deviation estimated using block averages over 10 time intervals.[36,37]

3. RESULTS: TIME-AVERAGED PROPERTIES

Interfacial Density and Thickness Are Similar for SPC/E and TIP4P/2005 Water and Depend on vdW Cutoffs. The time-averaged density profile of the water slab measured from its center of mass (at $z = 0$; see Figure 1 for the coordinate system used here) is shown in Figure 2 for both

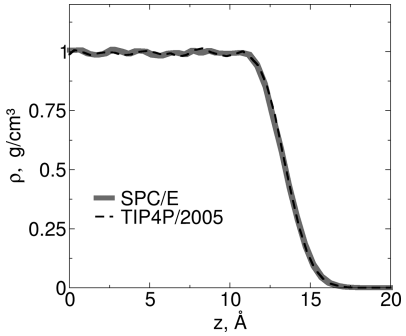

Figure 2. Average density of SPC/E and TIP4P/2005 water at each position in water slab. The standard deviation of the density at each z is on the order of the thickness of the gray line. As indicated in Figure 1, $z = 0$ corresponds to the center of mass of the water slab.

water models. The average density for the bulk region (defined as $z < 8$ Å) is $\rho_{SPC/E} = 0.995 \pm 0.008$ and $\rho_{TIP4P/2005} = 0.99 \pm 0.01$ g/cm^3. Within statistical uncertainty, both models reproduce the experimental density[38] $\rho_{300\ K} = 0.9965$ g/cm^3. The bulk densities obtained here also agree with reported values for the SPC/E and TIP4P models, as well as for the polarizable model TIP4P-POL2 for similar water slab geometries.[39] In contrast, neither the polarizable water model FLUC-q[39] nor the density functional theory based ab initio molecular dynamics (MD) employing the BLYP functional reproduces experimental density[9,10,20] (although the inclusion of a dispersion correction substantially improves the AIMD/BLYP approach).

As shown in Figure 2, calculation with either water model produces nearly identical space- and time-averaged density profiles that smoothly decrease from the bulk to zero over approximately 5 Å. A discussion of the origin of these profiles and the consequences of space and time averaging at the interface is offered below. To compare our interfacial density profiles quantitatively to prior reports,[11,40] we fit the data to a hyperbolic tangent:

$$\rho = a\left(1 + \tanh\left(-\frac{z - z_G}{\delta}\right)\right) \quad (1)$$

where z_G indicates the position at which the interfacial density is half of the bulk (i.e., the Gibbs dividing surface), a is approximately the average density of the liquid plus the vapor, and δ captures the interfacial thickness. Fitting the data shown in Figure 2 using equation eq 1 gives an interfacial thickness parameter that differs by 7% between models ($\delta_{SPC/E} = 1.49$ Å and $\delta_{TIP4P/2005} = 1.39$ Å), suggesting that differences in charge location between the two models have a small but measurable impact on interfacial thickness. The influence of the water model on the interfacial thickness parameter δ is not surprising, as prior work has shown this dependence: values of δ ranging from 50% smaller to 20% larger than those found here have been reported.[10,39] Interestingly, reported values[39] of the interfacial thickness parameter δ for SPC/E water, from simulations at the same temperature and using systems of similar size, are ≈4% larger than those found in this work. This difference likely arises from shorter cutoffs (12 Å, instead of 15 Å here) used for van der Waals interactions: preliminary simulations (not discussed here) performed by us using 12 Å cutoffs also resulted in a 3% increase in δ. These results indicate that models using short van der Waals cutoffs and parametrized to reproduce bulk properties must be carefully evaluated for their suitability to reproduce the properties of liquid interfaces, particularly in the case of weakly polar liquids where van der Waals interactions may be the predominant nonbonded interaction. Finally, we note that the relative insensitivity of the density profile to charge location on the water molecule agrees with a prior work demonstrating the relative insensitivity of the surface potential of the air/water interface to charge mobility (polarizability).[41]

Interfacial Water Population Can Be Identified from Time- and Space-Averaged Density and Hydrogen-Bond Profiles. By definition, interfacial water molecules have fewer neighbors than those in the bulk, so one would expect that they form fewer hydrogen bonds than in the bulk. We quantify this reduction by calculating the fraction of OH groups that do not donate a hydrogen bond (i.e., free OH groups) f_{fOH} at each position in the water slab:

$$f_{fOH}(z) = \frac{\langle n_{fOH}(z)\rangle}{\langle n_{OH}(z)\rangle} \quad (2)$$

The average numbers of free $\langle n_{fOH}(z)\rangle$ and total $\langle n_{OH}(z)\rangle$ OH groups at each position are calculated over all saved configurations (200 000). $f_{fOH} = 0$ when all OH groups at a given position donate a hydrogen bond, and 1 when none do. As might be expected, f_{fOH} depends strongly on hydrogen-bond criteria. To overcome this inherent ambiguity, we here use three criteria, ranging from strict to loose. Hydrogen bonds are present if the O···O distance is less than and the minimum O–H···O angle is greater than HB1 = (3.1 Å,160°), HB2 = (3.5 Å,140°), or HB3 = (4.0 Å,130°). HB1 is the strictest criterion, identifying only strong hydrogen bonds whereas HB3 is the loosest, capturing also very weakly hydrogen-bonded states.

The dependence of $f_{fOH}(z)$ on hydrogen-bond criteria is illustrated in Figure 3 for an SPC/E water slab. As expected, the strictest hydrogen-bond criterion (HB1) leads to a much higher fraction of free OH groups in the bulk and lower differences between the fraction of free OH groups in the bulk and at the interface than the looser HB2 and HB3 criteria. Despite the large differences in the $f_{fOH}(z)$ values for the three hydrogen-bond criteria, all show the same expected trend: f_{fOH} is significantly higher at the interface than in the bulk presumably

dx.doi.org/10.1021/jp304151e | J. Phys. Chem. B 2012, 116, 9467–9481

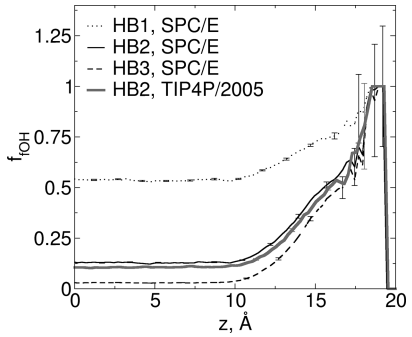

Figure 3. Fraction $f_{fOH}(z)$ of free OH groups at each position in the water slab (0 is the center) for SPC/E water, for three hydrogen-bond criteria. For comparison, the fraction of free OH groups for TIP4P/2005 water and the HB2 criterion is also shown. The error bars indicate the standard deviation.

because the interface limits the number of neighbors within hydrogen-bonding distance. A comparison of f_{fOH} values for the SPC/E and TIP4P/2005 models using the HB2 criterion is also shown in Figure 3. Similar to interfacial density, f_{fOH} is also apparently insensitive to the position of the charge on fixed charge water models.

The density and hydrogen-bond profiles presented in Figures 2 and 3 are used to define the interfacial and bulk regions. Bulk water is defined as the region where $z < 8$ Å for both water models, a sufficiently strict criterion to avoid interfacial effects because static and dynamic properties remain at their bulk values up to $z \approx 10$ Å. Similar to the bulk, the interface is also defined as a three-dimensional (3D) slab, but the lower z cutoff delimiting the interfacial region is obtained by imposing the condition that the fraction of free OH groups (HB2 criterion) is at least 10% larger than the bulk. These interface criteria were chosen because they yield good agreement between structural and dynamic properties of interfacial water from simulation and from sum frequency generation experiments, as discussed in more detail below and in a previous publication.[8] We note, however, that properties of interfacial water discussed in this paper are not sensitive to small changes in the interface definition (e.g., increasing the z cutoff for the interface by +1 Å, making the 3D interfacial slab 1 Å thinner, decreases the interfacial mass by 30%, but changes the average angle of the interfacial free OH groups with the surface normal by only 4%).

These criteria lead to slightly different interface boundaries for the SPC/E and the TIP4P/2005 water models: for SPC/E the interface is the region with $z > 10.51$ Å; for TIP4P/2005, it is $z > 10.32$ Å. For both models the interfacial thickness is thus approximately 5 Å. The residence time of waters at the interface is ≈10 ps for both models (see Supporting Information). As the structural and hydrogen-bond dynamics of interest are 5−10 times faster, we do not add an additional lifetime criterion to our definition of interfacial water.

Since our eventual interest lies in connecting our results with experiment, we must verify that our interface definition identifies the same population of water molecules investigated by surface-specific spectroscopic techniques such as VSF or second harmonic generation (SHG) spectroscopy. Much prior work at the pure water/air interface has shown that these techniques probe the top two water layers.[42−47] These layers are not visible in the density profiles shown in Figure 2 because of spatial and temporal averaging over surface capillary waves induced by thermal fluctuations.[11,48,49] Several methods now exist to filter out the effect of capillary waves,[11,40,50−52] enabling the calculation of the intrinsic surface density profiles, i.e., the surface density as a function of the distance to the topmost water layer. These profiles show two distinct water layers (before reaching bulk densities),[52] consistent with results from VSF or SHG spectroscopy. The two topmost interfacial water layers have a thickness of approximately 5 Å. As the time- and space-averaged criteria used in our work lead to the same interfacial thickness, it seems likely that the population of interfacial water we examine is the same as that probed in either VSF or SHG experiments.

f_{fOH} has been found experimentally, using time-averaged VSF spectroscopy, to be ≈0.2.[13,53] While a detailed comparison of our computed results to the VSF work is challenging—likely requiring direct calculation of the VSF spectral response and charge rearrangement[54]—less strict comparisons are possible. From the three hydrogen-bond criteria used in this study, HB2 leads to the best agreement with experiment: we find that 21% (TIP4P/2005) to 24% (SPC/E) of interfacial OH groups are free. In our more recent work exploring the dynamics of OH groups in their free state at the air/water interface, we also found that HB2 allowed for better replication of other experimental observables.[8] In the analysis that follows, then, we mostly use the HB2 criterion; when appropriate we use the other two criteria as well, to facilitate comparison with prior work.

Acceptor-Only Water Molecules at the Interface Are Not Abundant. Free OH groups may belong to water molecules where one or both OHs are free. We assess the magnitude of these two water subpopulations by calculating the fraction of water molecules with one or two free OHs at each position in the water slab. The results using the HB2 criterion, shown in the Supporting Information, indicate that water molecules with two free OH groups predominate only in the outer regions of the interface ($z > 17$ Å). As these regions have extremely low density, waters with two free OHs are not a significant interfacial population. These results are in quantitative agreement with prior studies using ab initio MD[10] and other classical models.[39] Both X-ray absorption spectroscopy[55] of water microjets and time-averaged VSF spectroscopy of the air/water interface[16] have similarly found that double free OH water molecules do not occur in significant numbers at the air/water interface. These results are consistent with the findings of Varilly[56] which indicate that water molecules evaporate by a rare event in which one water molecule sticks out of the interface and breaks the final hydrogen bond.

Interfacial Free OH Groups Preferentially Point Out of the Interface and Bonded Ones Lie Flat. The interface necessarily imposes a preferential orientation of free and hydrogen-bonded OH groups in the normal direction (OZ; see Figure 1). We characterize this preferential orientation by computing the probability density, $P_y(\theta)$, of finding free or bonded OH groups at an angle θ with the surface normal (see Figure 1 for the spherical coordinate system used here):

$$P_y(\theta) = \frac{\langle n_{y\mathrm{OH}}(\theta)\rangle}{\langle n_{y\mathrm{OH}}\rangle\, \delta\theta} \tag{3}$$

In eq 3 $\langle n_{y\mathrm{OH}}(\theta)\rangle$ is the average number of free (y = f) or bonded (y = b) OH groups in a given region (interface or bulk) with angle θ relative to the surface normal, $\langle n_{y\mathrm{OH}}\rangle$ is the average total number of free or bonded OH groups in that region, and

dx.doi.org/10.1021/jp304151e | J. Phys. Chem. B 2012, 116, 9467−9481

$\delta\theta$ is the bin width used in the histogram. This probability density is shown in Figure 4a; the corresponding effective

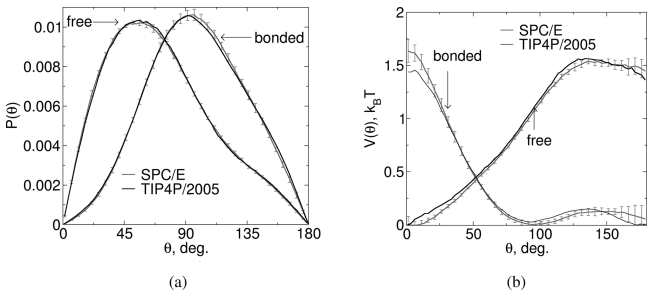

Figure 4. (a) Probability density $P(\theta)$ and (b) corresponding effective potential $V(\theta)$ of interfacial free or hydrogen-bonded OH groups (HB2 criterion) for SPC/E and TIP4P/2005 water. The statistical uncertainty is only shown for the SPC/E model for clarity but is similar for the TIP4P/2005.

potential (i.e., free energy landscape)[57] $V_y(\theta) = -k_B T \ln(P_y(\theta)/\sin(\theta))$ (shifted so that the minimum for each curve is zero) is shown in Figure 4b. Figure 4 indicates that both free and bonded OH groups at the interface have broad and non-sine-function orientation distributions, with free OH groups preferentially pointing out of the water slab and hydrogen-bonded OHs preferentially lying on the interface, in qualitative agreement with early SHG experiments.[58] The orientation distributions are almost identical for the two water models: the mode and standard deviation of the distribution of hydrogen-bonded OH groups (HB2 criterion) are $\theta = 94 \pm 40°$ (SPC/E) and $\theta = 93 \pm 39°$ (TIP4P/2005) (in each case with a significant skewness toward $\theta > 90°$); the same quantities for the distribution of free OH groups are $\theta = 56 \pm 41°$ (SPC/E) and $\theta = 57 \pm 40°$ (TIP4P/2005). Recent AIMD simulations show similar $P_f(\theta)$ distributions for the interfacial free OH groups, with an average $\theta = 56°$.[10] This agreement is likely coincidental because a different hydrogen-bond criterion was used in that work and, as shown in the Supporting Information, the shape and maximum of the $P_f(\theta)$ curves for the free OH groups depend on this parameter. In contrast to the free OH, the interfacial hydrogen-bonded OH orientation is independent of hydrogen-bond criteria (see Supporting Information for details). The maximum and width of the orientation distributions for the interfacial free OH groups quantitatively agree with results from time-resolved VSF experiments,[8] further confirming that the interface definition used here identifies the same interfacial population of water molecules as probed in those experiments.

Orientation of Interfacial Free and Bonded OH Groups Depends on Interfacial Position. Prior time-averaged VSF spectroscopy studies of the air/water interface have concluded that the orientational distribution of the free OH can be well described by a Gaussian distribution centered at ≈30° with a relatively narrow width ($\sigma = 15°$).[16] Clearly these numbers disagree with the free OH distribution shown in Figure 4a; these numbers are also inconsistent with recent results from time-resolved VSF[8] which, as mentioned above, agree well with our simulations. To investigate the origin of this disagreement, we ask if the orientation of all OH groups (free or hydrogen bonded) depends on their position along the interface normal (in z). We calculate the density $f_{yOH}(\theta,z)$ of OH groups at each position z that form an angle θ with the surface normal, according to

$$f_{yOH}(\theta, z) = \frac{\langle n_{yOH}(\theta, z)\rangle}{\langle n_{yOH}(z)\rangle\, \delta\theta} \tag{4}$$

Here $n_{yOH}(z)$ is the number of free (y = f) or bonded (y = b) OH groups at each position z and $n_{yOH}(\theta,z)$ is the number of free or bonded OH groups at the same position that form an angle θ with the surface normal. This choice of normalization highlights the preferential orientation of OH groups *at each z*: for each z, $f_{yOH}(\theta,z) = 0$ if no OH groups have a particular orientation θ and $1/\delta\theta$ if all OH groups at that z position point in a single direction. The probability density $f_{yOH}(\theta,z)$ is shown in Figure 5 for the HB2 criterion, but the observed trends are robust to changes of hydrogen-bond definition. Inspection of Figure 5 indicates that moving from the bulk toward the interface (increasing z) changes the orientation distribution of OH groups from broad and isotropic (i.e., a population centered at 90° in this spherical coordinate system) to two narrower distributions, centered at higher values of θ for the bonded OH groups and at low values for the free OH groups. For example, the mean and standard deviation of θ in the bulk are 90 ± 46°, but the same quantities in an outer interfacial 3D region with upper and lower boundaries $z = 16 \pm 0.125$ Å are 122 ± 24° for the hydrogen-bonded SPC/E OH groups and 37 ± 22° for the free OH groups. The change in θ of both populations as a function of position in the interface ($z > 10.32$ Å for SPC/E water) is in agreement with early computational

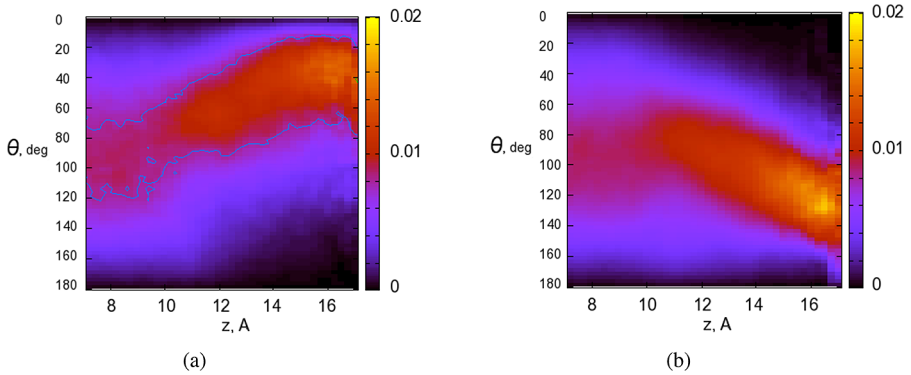

Figure 5. Probability density of (a) free ($f_{fOH}(\theta,z)$) and (b) bonded ($f_{bOH}(\theta,z)$) SPC/E OH groups at position z in the water slab which form angle θ with the surface normal. $f_{yOH}(\theta,z)$ is normalized by the number of free or bonded OH groups at each z, so the lower water density at the interface is not apparent in these plots. The HB2 criterion was used in both cases.

dx.doi.org/10.1021/jp304151e | J. Phys. Chem. B 2012, 116, 9467−9481

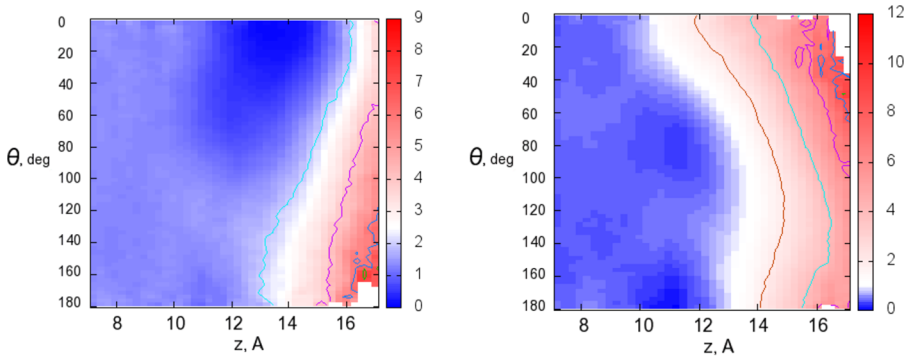

Figure 6. Effective potentials $V_y(\theta,z)/(k_BT)$ for (a) free and (b) bonded OH groups. Note that $V_y(\theta,z)$ is normalized by the total number of OH groups in each histogram, so these plots account for the lower water density at the interface. The HB2 criterion was used in both cases.

Table 1. Mean and Standard Deviation of the Distance d and Angle φ, Shown as $(\mu_d \pm \sigma_d,\mu_\varphi \pm \sigma_\varphi)$, That Characterize the Hydrogen-Bonded State of an OH Group of the SPC/E and TIP4P/2005 Water Models

location	SPC/E	TIP4P/2005
interface	(2.792 ± 0.146,162.6 ± 11.2)	(2.823 ± 0.143,162.9 ± 11.0)
bulk	(2.782 ± 0.142,163.1 ± 10.9)	(2.808 ± 0.137,163.4 ± 10.7)

studies of the air/water interface.[18] Similar changes of orientation as a function of position were also observed in recent studies of water near an extended hydrophobic interface,[59] as discussed in detail in the Supporting Information, confirming the (expected) similarity between the air/water and hydrophobic/water interfaces.

The peak and width of the orientation of the free OH groups from time-averaged VSF (30 ± 15°) clearly agree much better with those values for the outer free OH groups (37 ± 22°, as shown above for z = 16 Å) than for the full interfacial free OH population (for SPC/E water, θ = 56 ± 41° for z > 10.32 Å as discussed above). This suggests that time-averaged VSF studies probe only the outer OH groups instead of the two outer water layers. Since the time scales over which the free OH average orientation changes are on the order of the vibrational dephasing time, time-averaged VSF measurements preferentially sample longer-lived groups.[8] We have previously reported that longer-lived free OH groups have smaller average values of θ and a narrower orientational distribution (see also the Supporting Information); Figure 5a shows that OH groups with smaller average values of θ are in fact closer to the vapor phase. In contrast, time-resolved VSF studies that sacrifice spectral resolution for greater signal size do not bias toward long-lived interfacial free OH groups.[8] The observed agreement between the peak and width of the free OH distributions shown in Figure 4a and results from time-resolved VSF experiments, and between the peak and width of the distributions of the topmost water molecules and results from time-averaged VSF experiments, indicates that different techniques probe different interfacial water populations.

Movement of Free and Bonded Interfacial OH Groups Occurs in an Effective Potential. Taken together, Figures 2, 4, and 5 indicate that movement of either free or bonded OH groups—and transitions between these states—at the interface occurs within two-dimensional effective potentials $V_y(\theta,z)$. These potentials can be expressed as

$$V_y(\theta, z) = -k_BT \ln\left(\frac{\langle n_{yOH}(\theta, z)\rangle}{\langle n_{yOH}(z)\rangle \sin\theta}\right) \quad (5)$$

where n_{yOH} is the number of free or bonded OH groups. These potentials (shifted so that the minimum is zero) are shown in Figure 6 for the SPC/E model and the HB2 criterion. At the interface, bonded OH groups have a broad free energy minimum at 10 < z < 12 Å and 60 < θ < 180°; free OH groups have a comparatively narrower minimum further into the vapor phase, at 12 < z < 14 Å and 0 < θ < 60°. Below we examine transitions between the free and bonded states at the interface and relate the characteristic relaxation time of each population to the free energy landscapes shown in Figure 6.

Hydrogen Bonds at the Interface Are Slightly Stronger Than in the Bulk. The hydrogen-bonded state of an OH group is well-described by a two-dimensional probability density $P_{HB}(d,\varphi)$ with reaction coordinates of the O···O distance d and the O−H···O angle φ (with vertex at the H atom) between an OH group and its oxygen acceptor. As interfacial OH groups are anisotropically oriented in θ, it is reasonable to ask whether the interface modifies the $P_{HB}(d,\varphi)$ distribution relative to water in the bulk. Prior reports indicate that such changes reflect differences in hydrogen-bond strength.[60−62] Note that the expression "hydrogen-bond strength" here means the strength of the pair interaction between two water molecules that share a hydrogen bond. Stronger hydrogen bonds have been shown to correlate with lower frequencies of vibration of the O−H bond and with slower rotational dynamics of water for time scales up to 1 ps, but they have no impact on the frequency of hydrogen-bond exchange (i.e., the hydrogen-bond lifetime) or on the rotational dynamics of water at longer time scales.[61]

We compute two-dimensional (d,φ) histograms separately for water pairs in which the central water molecule is either at the interface or in the bulk, using as distance and angle cutoffs the loosest HB criterion (HB3). Employing the loosest H-bond criterion for this purpose suggests that we will see the largest possible difference between the bulk and interfacial hydrogen-bonded states: as more weak hydrogen bonds will be included

dx.doi.org/10.1021/jp304151e | J. Phys. Chem. B 2012, 116, 9467−9481

in the comparison, any differences in the probability distribution $P_{HB}(d,\varphi)$ due to the population of weak hydrogen bonds will be detected. The $P_{HB}(d,\varphi)$ histograms are shown in the Supporting Information. We determine the mean μ and the standard deviation σ of d and φ by fitting a bivariate Gaussian distribution to the histograms as described in the Supporting Information. We find that the mean distance and angle associated with a hydrogen bond, shown in Table 1, are similar at the interface and in the bulk for both water models: μ_d is less than 0.5% larger and μ_φ is 0.3% smaller at the interface than in the bulk. As discussed in further detail in the Supporting Information, these results qualitatively agree with reported experiments and ab initio MD simulations.[10,39,55,60,63] The lower mean φ at the interface observed here indicates that hydrogen bonds become more bent, an effect which contributes to weaker interfacial hydrogen bonds than in the bulk.[62] In contrast, the larger mean O···O distance for water at the interface strengthens interfacial hydrogen bonds relative to bulk ones. This strengthening occurs because μ_d at the interface is closer to the O···O distance at the global energy minimum for a water dimer[62] than μ_d in the bulk. These differences in mean O···O distance and O−H···O angle between the bulk and the interface have opposing contributions to hydrogen-bond strength, suggesting that hydrogen bonds at the interface should have strength similar to that in the bulk. Indeed, prior work by Jedlovszky confirms that interfacial hydrogen bonds are only slightly stronger than hydrogen bonds in the bulk, with the interaction energy between SPC/E water molecules at the air/water interface and their hydrogen-bonded neighbors being approximately 10% more negative than in the bulk.[60] As mentioned above, prior work by Laage and Hynes has shown that such a small change in hydrogen-bond strength will not have noticeable effects on the reorientation dynamics of OH groups.[61] We conclude that changes in hydrogen-bond strength are not behind the differences between water at the interface and in the bulk described below with respect to either reorientation dynamics or frequency of hydrogen-bond exchange.

4. RESULTS: REORIENTATIONAL DYNAMICS

Overall Reorientational Dynamics of OH at the Interface Is Slightly Faster Than in the Bulk. We characterize the rotational motion of OH groups using a second order rotational autocorrelation function of the form

$$P_2(\tau) = \left\langle \frac{1}{2}(3\cos^2(\vec{u}_0\cdot\vec{u}_\tau) - 1) \right\rangle \quad (6)$$

where $\vec{u}$ is the unit vector characterizing the orientation of an OH group (with respect to the coordinate frame given in Figure 1) and the average is over all time origins. The function's maximum, 1, occurs with perfect orientation correlation; its minimum of −0.5 is reached if all OH groups are orthogonal to their initial orientation; $P_2 = 0$ in the limit of perfect (i.e., isotropic, 3D) decorrelation.[64]

The reorientation dynamics of OH groups in the bulk and at the interface, as measured by P_2, are shown in Figure 7. The curves include only those OH groups that are at the same location (interface or bulk) at both $t = 0$ and $t = \tau$. Inspection of Figure 7 shows several qualitative features of the dynamics: all curves have an initial nonexponential decay ($\tau < 0.2$ ps; see inset of Figure 7) followed by a quasi-exponential one. The short-time decay comprises two parts: a very fast decay ($\tau <$ 100 fs) followed by underdamping ($100 < \tau < 200$ fs). These qualitative characteristics of water dynamics have been previously described in bulk water and (through sampling of a dipole moment orientational correlation function) at the air/water interface, and appear to be insensitive to the water model.[39] Overall, reorientational relaxation is slightly faster at the interface than in the bulk for both models. This conclusion agrees with prior studies employing a variety of classical fixed charge (including SPC/E), classical polarizable, and AIMD water models that have also found water at the air/water interface experiences faster reorientational relaxation than water in the bulk.[10,39] Finally, it is clear that SPC/E water undergoes faster dynamics than TIP4P/2005 water.

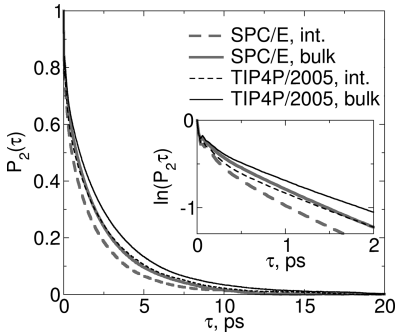

Figure 7. Reorientation dynamics of OH groups at the interface or in the bulk for SPC/E and TIP4P/2005 water, as measured by $P_2(\tau)$. The standard deviation of $P_2(\tau)$ is on the order of the thickness of the lines. The corresponding decay times are given in Table 2. The inset shows $\ln(P_2)$ between 0 and 2 ps.

To gain additional insight, we fit the curves in Figure 7 with a biexponential of the form $P_2(\tau) = a\exp(-t/b) + c\exp(-t/\tau_r)$, where b is a fast decay time and τ_r is the long-time characteristic reorientation decay time. Even though the short-time decay is clearly nonexponential as shown in the inset of Figure 7, because the nonexponential region is narrow, the biexponential function results in a good overall fit of the data. The short decay times vary between 0.2 and 0.4 ps, depending on the water model or position in the water slab, and reflect the expected short-time librational motion of the OH groups. In this work we focus on the long-time reorientation of OH groups, characterized by the reorientation times given in Table 2. The

Table 2. Reorientation Decay Times τ_r (ps) for the Two Water Models, for OH Groups either at the Interface or in the Bulk[a]

location	SPC/E	TIP4P/2005
interface	2.31	2.91
bulk	2.63	3.25

[a]The uncertainty of τ_r is ±0.01 ps (asymptotic standard error of the fit).

SPC/E water model leads to a reorientation time for water in the bulk that compares very well with that for the OD bond in HOD/H_2O obtained from polarization resolved infrared transient absorption, NMR, and dielectric relaxation spectroscopies at 300 K ($\tau_{r,exp}$ = 2.0−2.5 ps); in contrast, the TIP4P/2005 water model has somewhat slower reorientation dynamics than indicated by experiment.[4,67,68] In both models, and in agreement with most earlier studies, reorientation at the interface is slightly faster than in the bulk: the interfacial

dx.doi.org/10.1021/jp304151e | J. Phys. Chem. B 2012, 116, 9467−9481

orientational relaxation times are slightly smaller (SPC/E, 12%; TIP4P/2005, 10%) than those in the bulk (see Table 2). We note that the decrease in reorientation relaxation times at the interface relative to the bulk observed here apparently conflicts with the 3-fold decrease reported for the dipole reorientation times from AIMD simulations.[10] However, because of the relatively small system sizes possible in current AIMD simulations, the statistical uncertainty associated with determining the characteristic time of the dipole orientation autocorrelation function in that work is large. In the absence of further AIMD simulations, it is difficult to conclude whether these differences are due to differences in the underlying physical representation of water.

We emphasize that even for $\tau > 0.5$ ps the reorientation decay is only quasi-exponential. This result is consistent with different subpopulations of OH groups reorienting through different mechanisms. Such dynamic heterogeneity is expected, both at the interface and in the bulk: in the bulk, the reorientation of hydrogen-bonded OH groups is known to be well-described by two processes[21,69] (discussed in more detail below); at the interface, free OH groups experience a dramatically different energy landscape than hydrogen-bonded ones so it it perhaps reasonable that their dynamics differ from hydrogen-bonded OH groups as well. The origin of dynamic heterogeneity for water at the interface is discussed in much more detail in the remainder of the paper.

Population of Free OH Groups Is Abundant and Long-Lived Only at the Interface. To understand the origin of dynamic heterogeneity, it is useful to compare the reorientation mechanism(s) at the interface to bulk. Before doing so we wish to briefly clarify what we mean when we write "the mechanism of water reorientation in the bulk". The potential problem here is that, as is apparent in the results plotted in Figure 3, both hydrogen-bonded and free OH groups exist in the bulk (although the relative amounts depend on the hydrogen-bond definition). The population of free OH groups in bulk water has two important characteristics: it is small (as shown above) and it has much shorter lifetimes than the hydrogen-bonded OH groups (as shown in Table 3 for the SPC/E water model; see Supporting Information for details of the calculation). It is therefore not surprising that the reorientational dynamics of bulk OH groups in this environment can be rationalized in terms of *hydrogen-bonded* OH groups only.[21,69] In contrast, at the air/water interface the population of free OH groups is significantly larger and these groups have on average longer lifetimes (Table 3), so as expected, understanding the loss of orientational correlation of OH groups at the interface requires that both free and bonded interfacial OH subpopulations are considered.

Table 3. Lifetimes (ps) of Free or Bonded (HB2 Criteria) OH Groups for the SPC/E Water Model[a]

	free	bonded
interface	1.09	3.94
bulk	0.29	4.17

[a]The statistical uncertainty of the reported lifetimes is 0.02 ps (asymptotic standard error of the fit).

Hydrogen-Bond Exchange at the Air/Water Interface. *Mechanism of Hydrogen-Bond Exchange Is Identical at the Interface or in the Bulk.* For water in the bulk, Hynes and co-workers have shown[21,69] that the loss of orientational correlation is almost entirely due to two processes: large-amplitude jumps between stable hydrogen-bonded states (i.e., hydrogen-bond exchange) and diffusive reorientation of the bonded OH groups in between jumps (i.e., the reorientation of the O−H···O system as a whole, called the "frame reorientation"). In what follows we look at these processes for bulk and interfacial hydrogen-bonded OH groups and evaluate their contribution to the loss of orientation correlation as measured by P_2 (Figure 7).

In the bulk, the mechanism of hydrogen-bond exchange involves a simultaneous increase of the distance between the oxygen donor and the initial (here called "old") oxygen acceptor ($O_d\cdots O_o$), a decrease in the distance between O_d and the new oxygen acceptor ($O_d\cdots O_n$), and a rapid angular jump described by the angle ϑ (see Supporting Information for a cartoon representation of the process) during which the rotating OH group breaks its hydrogen bond with O_o and establishes a new one with O_n. We assess how hydrogen-bond exchange at the interface differs from that in the bulk by comparing the sequence of events involved in this process (the change in the $O_d\cdots O_o$ and $O_d\cdots O_n$ distances and in angle ϑ) for hydrogen-bond exchange in both locations. We do so using the stable states picture of reactions,[70] following Hynes and co-workers:[21,71] we analyze only jumps between stable hydrogen-bonded states (defined as those that meet the stringent HB1 criterion) to avoid recrossing of the free energy barrier between states. We find that the mechanism of hydrogen-bond exchange is identical at the interface and in the bulk. This is illustrated in the Supporting Information, where the average and non-averaged trajectories in the angle ϑ and the distances $O_d\cdots O_o$ and $O_d\cdots O_n$ for hydrogen-bond exchange in SPC/E water are shown. Very similar curves—not shown—are obtained for the TIP4P/2005 model. Clearly, hydrogen-bonded interfacial OH groups undergo an angular jump during hydrogen-bond exchange that is identical in every way to that described by OH groups in the bulk.

Frequency of Hydrogen-Bond Exchange Is Slower but O−H···O Frame Reorientation Is Faster at the Interface Than in the Bulk. We show in the Supporting Information that hydrogen-bonded OH groups at the air/water interface experience an essentially identical large-amplitude angular jump as hydrogen-bonded OH groups in the bulk. We now address the question of whether jump frequency or the frame rotation rate changes between the two environments and whether, if these processes are accounted for properly, they are responsible for the slightly faster OH reorientation at the interface shown in Figure 7. Hynes and co-workers[21,69] have previously demonstrated that the P_2 for water in the bulk and around small solutes can be modeled through application of the Ivanov jump model[72] and by assuming that OH rotation between jump events occurs diffusively. The resulting equation is[73]

$$\frac{1}{\tau_r} = \frac{1}{\tau_{ex}}\left[1 - \frac{1}{5}\frac{\sin\left(\frac{5\Delta\vartheta}{2}\right)}{\sin\left(\frac{\Delta\vartheta}{2}\right)}\right] + \frac{1}{\tau_f} \quad (7)$$

To actually solve equation eq 7, we require $\Delta\vartheta$ (64°; see Supporting Information), τ_{ex}, and τ_f from simulation.

Obtaining the Frame Decay Time. In practice, τ_f is estimated by calculating $P_2(\tau)$ for the subpopulation of OH groups that at time τ are in the same region (interface or bulk) and donate a hydrogen bond (HB1 criterion) to the same

acceptor oxygen as at $t = 0$. Similarly to what was observed for the full reorientation decay shown in Figure 7, the frame reorientation (shown in the Supporting Information) shows a short-time, nonexponential decay followed by a quasi-exponential regime; the full curve is well-approximated by a biexponential function. As the uncertainty of the frame decay increases considerably for larger times, the weight of each data point in the fit is given by its associated uncertainty. We find that the short decay times are <0.5 ps and are associated with fast oscillations of the OH groups; the diffusive reorientation of the frame is described by the longer decay time, τ_f. Inspection of the resulting frame decay times (see Table 4) clarifies that

Table 4. Frame Decay Times τ_f and Hydrogen-Bond Exchange Time τ_{ex} (ps) for the Two Water Models, for OH Groups That at $t = 0$ Are either at the Interface or in the Bulk[a]

	location	SPC/E	TIP4P/2005
τ_f	interface	4.53	5.70
	bulk	5.75	7.17
τ_{ex}	interface	3.779	4.572
	bulk	3.163	3.681

[a]The uncertainty of τ_f is ±0.04 ps and that of τ_{ex} is ±0.002 ps (asymptotic standard error of the fit).

frame reorientation is approximately 20% faster at the interface than in the bulk. The faster frame reorientation at the interface likely arises from the faster translational dynamics (see Supporting Information) observed in that region; faster translation facilitates rotational diffusion of O−H···O as a whole.

Obtaining the Time between Jumps. We define the characteristic time between jumps τ_{ex} (also called the "jump time") from the cross-correlation function $C(\tau)$:

$$C(\tau) = \langle n_R(0)\, n_P(\tau)\rangle \quad (8)$$

By definition, $n_R(0) = 1$ if a particular OH group donates a stable hydrogen bond (HB1 criterion) and belongs either to the interface or to the bulk at time zero; $n_R(0) = 0$ otherwise. $n_P(\tau) = 1$ from the instant τ in which the same OH group establishes a different, stable, hydrogen bond (i.e., absorbing boundary conditions are used in the product); $n_P(\tau) = 0$ otherwise. Explicitly requiring that the product state remains in the same region (interface or bulk) at $t = t$ that it belonged to at $t = 0$ is not necessary because, since the residence times in the interface or the bulk are larger than the characteristic time between jumps, that condition is already met. The average is over all nonzero $n_R(0)$. $C(\tau)$ has its minimum value of 0 at $\tau = 0$ (all original reactant states are still present) and has a maximum value of 1 at long times, when all original hydrogen bonds have exchanged. The jump time τ_{ex} is the characteristic decay time of $C(\tau) = 1 - \exp(-t/\tau_{ex})$. Similar to the full and the frame reorientation decays, this function also shows nonexponential decay at short times followed by quasi-exponential decay at long times, so we again fit it with a biexponential and take the longer decay time of the two as τ_{ex}. The time between jumps for SPC/E water at the interface or in the bulk extracted from the fits is given in Table 4. Even though the jump mechanism is identical for water at the interface or in the bulk, jumps at the interface are less frequent than in the bulk by a factor of $\tau_{ex,int}/\tau_{ex,bulk} = 1.2$.

Slowdown of Hydrogen-Bond Exchange at the Interface Is a Transition State Excluded Volume Effect. An increase in the time between jumps was previously observed for water of hydration near small hydrophobic[71] or amphiphilic[23,74] solutes and also near larger idealized hydrophobic surfaces.[59] Interestingly, the retardation factor for hydrogen-bonded OH groups at the air/water interface is closer to that observed for water near small hydrophobic solutes (1.2) than for water near extended hydrophobic interfaces (1.8).[21,59] In those cases, it was possible to understand the origin of the slowdown by applying the transition state theory formalism to the hydrogen exchange process. During hydrogen-bond exchange, the system goes from a reactant state (the original hydrogen bond) to a product state (a different, stable, hydrogen bond) via a transition state. For hydrogen-bond exchange the transition state is the configuration, denoted by "†", where $O_d\cdots O_o = O_d\cdots O_n = R^\dagger$ and the rotating OH group is halfway between O_o and O_n ($\vartheta = 0$). For water near solutes, it was shown that retardation resulted from a decrease in the number of available transition state configurations as illustrated in Figure 8a, and the retardation factor could be accurately predicted from the fraction of excluded transition state configurations, f: $\tau_{ex}/\tau_{ex,bulk} = 1/(1 - f)$.[59,71]

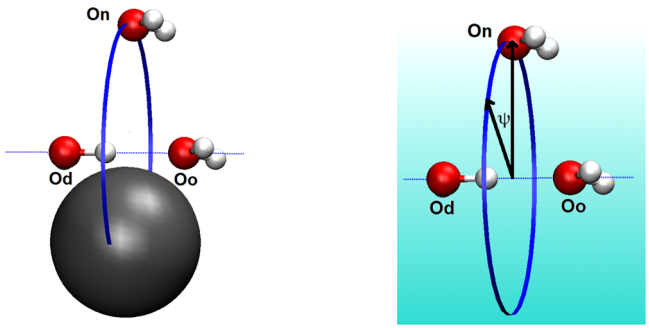

Figure 8. Possible transition state configurations for hydrogen-bond exchange between O_o and O_d. They are those on the blue ring defined by the distance $O_d\cdots O_n = R^\dagger$ and the angle $\angle O_o\cdots O_d\cdots O_n = \Delta\vartheta$. (a) For waters near a solute (gray sphere), the only available transition state configurations lie on the visible part of the ring. Near a sharp water−solute interface like this, the fraction $\bar{f}$ of available transition state configurations is the visible part of the ring divided by the total ring perimeter. (b) For waters at a finite thickness interface, the fraction $\bar{f}$ of available transition state configurations reflects the continuously varying time-averaged water density (here indicated by the light blue gradient) at different positions in the ring as described in the text.

An analogous reduction in the available transition state configurations must also occur for rotating waters at the air/water interface due to the termination of the water layer, but our results indicate that the theoretical retardation factor of 2 associated with a sharp, flat interface (for which the excluded volume fraction is 0.5) greatly overestimates the actual value of 1.2. The smaller retardation factor at the air/water interface suggests that the interface's finite thickness and its lower, but nonzero, time-averaged density relative to the bulk—depicted in cartoon form in Figure 8b—play a role in the observed rotational slowdown. We thus calculate a theoretical retardation factor accounting for these interfacial characteristics. For a single OH group that undergoes hydrogen-bond exchange and is at position z in the interface, the fraction of available

dx.doi.org/10.1021/jp304151e | J. Phys. Chem. B 2012, 116, 9467−9481

transition state configurations $\overline{f}(z) = 1 - f(z)$ (where f is the fractional excluded transition state volume and is also a function of z) relative to the bulk is calculated as the average density of water on the ring of possible transition state configurations (here sampled over 180 evenly spaced points on the ring) and normalized by the bulk water density:

$$\overline{f}(z) = \frac{\int_0^{2\pi} \rho(z + R^{\dagger} \sin(\Delta\vartheta) \cos(\psi))\, d\psi}{2\pi\rho_{bulk}} \quad (9)$$

The density at each position on the ring, $\rho(z_{ring}) = \rho(z + R^{\dagger} \sin(\Delta\vartheta) \cos(\psi))$ (ψ is defined in Figure 8b) is obtained from eq 1. Note that this definition of the fraction of available transition state configurations becomes equivalent to that proposed by Hynes and co-workers for the case of sharp interfaces because under those conditions $\rho(z_{ring})$ is either 0 or ρ_{bulk}. The average fraction $\langle\overline{f}\rangle = 1 - \langle f\rangle$ of available transition state configurations at the interface is then the average of the fraction of available transition state configurations at different heights in the interface, $\overline{f}(z)$, weighted by the density at height z:

$$\langle\overline{f}\rangle = \frac{\int_{z_i}^{z_f} \overline{f}(z)\, \rho(z)\, dz}{\int_{z_i}^{z_f} \rho(z)\, dz} \quad (10)$$

where z_i is the lower interface boundary (TIP4P/2005 = 10.32 Å; SPC/E = 10.51 Å) and z_f = 20 Å is the upper one. Using eqs 9 and 10, we find average excluded volumes $\langle f_{SPC/E}\rangle = 0.285$ and $\langle f_{TIP4P/2005}\rangle = 0.258$ which result in retardation factor values of $1/\langle\overline{f}\rangle = 1.40$ for the SPC/E model and $1/\langle\overline{f}\rangle = 1.34$ for TIP4P/2005. The calculated retardation factors agree well with those taken directly from the characteristic times between jumps (1.2 for both water models, as described above). The quality of the agreement indicates that the excluded volume model—proposed initially by Laage and Hynes[71] to explain the slowdown of rotation of water near hydrophobic interfaces—still holds for the case where an interface with non-negligible capillary waves is treated in a time- and space-averaged manner. These results indicate that the less marked slowdown of hydrogen-bond exchange for water at the air/water interface relative to water at extended hydrophobic/water interfaces is a direct consequence of larger-amplitude capillary waves at the air/water interface.

Hydrogen-Bond Exchange Alone Does Not Explain Faster Reorientation Decay at the Interface. Using the calculated values of $\Delta\vartheta$, τ_{ex}, and τ_f for the interface and the bulk and eq 7 we can estimate the reorientation time, $\tau_{r,est}$, of hydrogen-bonded OH groups in these two locations. Note that this reorientation time reflects only hydrogen-bond exchange; it does not account for bonded-to-free transitions that are non-negligible at the interface. For SPC/E water, these times are $\tau_{r,int,est} = 2.216 \pm 0.001$ ps and $\tau_{r,bulk,est} = 2.224 \pm 0.001$ ps; for TIP4P/2005, $\tau_{r,int,est} = 2.733 \pm 0.001$ ps and $\tau_{r,bulk,est} = 2.626 \pm 0.001$ ps. The statistical uncertainty of each estimated value was calculated using standard error propagation. Several points can be made by comparing the modeled reorientation decay times from hydrogen-bond exchange with the directly measured decay times (shown in Table 2) for the entire OH population at the interface or in the bulk. First, the modeled reorientation decay times at the interface are similar to the bulk values (they differ by 0.008 ps for the SPC/E water model and 0.107 ps for TIP4P/2005), despite the large differences in the characteristic hydrogen-bond exchange and frame decay times (0.5−1.5 ps; see Table 4). This similarity indicates that the faster frame rotation for interfacial hydrogen-bonded OH groups is largely compensated for by the smaller jump frequency. Second, the modeled decay times in the bulk differ no more than 0.6 ps from the directly measured decay times (shown in Table 2), indicating (as expected)[21] that the Ivanov model largely explains OH orientational relaxation in the bulk. Finally, whereas the directly measured decay times are larger in the bulk, the modeled ones show the opposite trend for TIP4P/2005 water or are almost identical in the bulk and at the interface for SPC/E water. If the decay of the interfacial P_2 summing over all water molecules (shown in Figure 7) was dominated, as in the bulk, by the reorientation of hydrogen-bonded OH groups, we would not expect this discrepancy. These results are consistent, however, with a scenario in which faster rotating interfacial free OH groups also contribute to the total interfacial P_2. In a quest for this faster rotating population, we next investigate the reorientational dynamics of the free OH groups in more detail.

Reorientation of Free OH Groups and Transitions between Free and Bonded States. To examine transitions between free and hydrogen-bonded states, we again use the stable states picture of reactions. As mentioned above, stable hydrogen-bonded states are identified using the HB1 criterion, corresponding to strong hydrogen bonds. Analogously, stable free states are those that do not establish even weak hydrogen bonds; as such they are identified using the HB2 criterion.

Reorientation Decay of Free, Interfacial OH Groups Is Faster than Overall Reorientation in the Bulk. The loss of orientation correlation of free OH groups at the interface as quantified by $P_2(\tau)$ (eq 6) is shown in a logarithmic scale in Figure 9; for comparison, the same plot includes the reorientation decay for water in the bulk which, as demonstrated above, reflects predominantly the reorientation of hydrogen-bonded OH groups through frame diffusion and hydrogen-bond exchange. The reorientation decay of the free, interfacial OH groups shows features similar to those already seen in the reorientation decay of the full interfacial (or bulk) OH populations: an initial fast decay due to librational motion, underdamping, and a subsequent quasi-exponential decay. Restricting ourselves to time scales of structural change ($\tau >$ 200 fs), inspection of Figure 9 shows two distinct regimes: from 0.2 to 1 ps reorientation of the interfacial free OH occurs at a higher rate than for bulk OH (as indicated by a steeper slope in

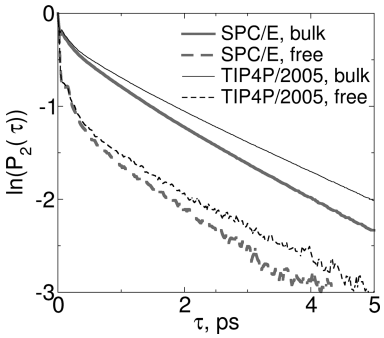

Figure 9. Reorientation decay as measured by $\ln(P_2)$ for the entire population of OH groups that at both $t = 0$ and $t = \tau$ belong to the bulk (repeated from Figure 7 to facilitate comparisons), or only for those that are free (HB2 criterion) and at the interface at both times.

dx.doi.org/10.1021/jp304151e | J. Phys. Chem. B 2012, 116, 9467−9481

the log plot) while for times greater than 1 ps it occurs at a comparable rate (the $\ln(P_2)$ curves for OH groups in the bulk or free OH groups at the interface are almost parallel). We and others have previously shown using simulation and VSF spectroscopy that this population of OH groups reorients more rapidly than OH in the bulk for time scales up to 1 ps.[8] Our current simulation results complement this picture and indicate that at longer time scales the rate of reorientation of free, interfacial OH groups slows down. The slower decay at longer times is the result of interfacial free OH approaching complete orientational randomization more slowly than other water species due to its time-averaged anisotropic orientation in θ (see Figure 4a).

Free OH Groups Reorient Diffusively. The results in Figure 9 suggest that the mechanism by which free OH groups reorient may be different from that for the bonded ones. In our previous study,[8] we addressed this question for subpicosecond time scales. There we found that free OH groups at the interface reorient diffusively, in contrast to the large-amplitude jump mechanism through which bulk OH groups reorient. Here we extend the analysis of the reorientation mechanism of free, interfacial OH groups for the case of extended vdW cutoffs and also TIP4P/2005 water. Because the interfacial free OH has a time-averaged anisotropic distribution only with respect to θ—it is isotropic with respect to ϕ (see the spherical coordinate system shown in Figure 1)—it is convenient to analyze its dynamics by considering movement in ϕ and θ separately. In this spirit, we characterize the in-plane (i.e., ϕ) motion of free OH groups by calculating the in-plane mean squared angular displacement (MSAD; $\langle\phi(t)^2\rangle$) and comparing it to the full MSAD ($\langle\omega(t)^2\rangle$) for water in the bulk (see Mazza et al.[75,76] and Supporting Information for details of the calculation).[77]

In the diffusive limit a plot of MSAD vs time on a log/log scale is linear with a slope of 1.[78] As shown in Figure 10 for

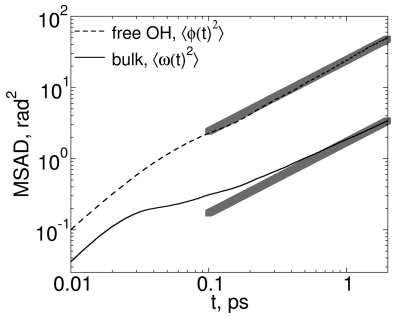

Figure 10. In-plane MSAD $\langle\phi(t)^2\rangle$ of free OH groups at the interface and full MSAD $\langle\omega(t)^2\rangle$ for all OH groups in the bulk for SPC/E water. The thicker lines illustrate the diffusive limit.

SPC/E water (results for TIP4P/2005 water are almost identical and so are not shown), for time scales comparable to the lifetime of the bonded or free OH groups at the interface the MSAD of bulk OH groups, $\langle\omega(t)^2\rangle$, is, as expected, nondiffusive.[21,69] Clearly the in-plane reorientation of the free OH during this time window, $\langle\phi(t)^2\rangle$, is much closer to the diffusive regime. This proximity to the diffusive limit indicates that free OH groups at the interface do not reorient by making fast and large-amplitude jumps in ϕ; i.e., their reorientation in ϕ is not an activated process.

As mentioned above, movement along θ takes place within an effective potential. Under these conditions, an MSAD plot with a slope of 1 in a log/log scale is not produced for diffusive motion. Instead, the MSAD in θ should quickly plateau,[79] as indeed happens for the interfacial free OH groups (see our previous study[8]). However, the nature of the effective potential in θ (and z) for free OH groups shown in Figure 6a suggests that movement in θ of this OH population should be diffusive: the observed effective potential landscape does not show any free energy barriers (i.e., it varies monotonically in θ) and is not very rugged (for the more populated regions of the interface, free energy differences along θ are $<2k_BT$). However, comparison of the distributions (Figure 5) and effective potentials (Figure 6) for free and bonded OH groups suggests, as mentioned above, that movement along θ may correlate with transitions between free and bonded states, because free OH groups point preferentially out of the interface and hydrogen-bonded ones point preferentially in. If these transitions occur through large-amplitude jumps that occur much faster than the characteristic time between jumps, then it is possible that a free energy barrier exists between free and bonded states and that the movement of free OH groups along θ is not necessarily diffusive at time scales comparable to that characteristic time. To investigate these issues, we examine transitions between free and hydrogen-bonded states in more detail.

Free-to-Bonded Transition Rate Slows Down at the Interface but the Bonded-to-Free One Remains Identical to Bulk. We first investigate trajectories in θ and z associated with free-to-bonded transitions at the interface. Rotation in θ and translation in z are investigated by looking at the distribution of θ angles or z positions as a function of the time relative to the instant (defined as $t = 0$) at which a (previously free) OH group first forms a hydrogen bond. These distributions are shown in Figure 11 for SPC/E water and the HB2 criterion; the distribution for TIP4P/2005 water (not shown) is almost identical. Several points can be made from these distributions. First, changes in the hydrogen-bonding state at the interface correlate with changes in z and θ, in agreement with the free energy landscapes shown in Figure 6: during a free-to-bonded event OH groups move closer to and reorient into the bulk. This movement is clearly visible in the transition to larger values of θ and smaller values of z (i.e., from outer to inner interfacial positions) for $t > 0$ in Figure 11a. However, whereas free-to-bonded transitions involve large-amplitude rotation in θ (in Figure 11a, from −0.15 to 0.15 ps θ changes on average 35°), they involve comparatively smaller changes in z (in the same time interval z changes on average only 0.4 Å). Second, the z and θ distributions before and after $t = 0$ substantially overlap, suggesting that changes in the hydrogen-bonding state should be largely diffusive. Third, the actual free-to-bonded event lasts a minimum of 0.3 ps (see Figure 11a). As mentioned above, comparison of this time to the characteristic time between successive individual free-to-bonded ($\tau_{f,b}$) or bonded-to-free transitions ($\tau_{b,f}$) offers further insight into the mechanism (diffusive or not) of the change of the hydrogen-bond state at the interface: if $\tau_{b,f}$ and $\tau_{f,b}$ are much larger than 0.3 ps, changes of the hydrogen-bond state are activated processes; if the opposite, they are predominantly diffusive.

We calculate the times $\tau_{f,b}$ and $\tau_{b,f}$ through a $C(\tau)$ function analogous to eq 8 but with different definitions of reactant (free or bonded) and product (bonded or free) states. The functions $C(\tau)$ obtained for free-to-bonded and bonded-to-free transitions are well fitted by biexponentials, similarly to what we show above for hydrogen-bond exchange. However, whereas for hydrogen-bond exchange the exponential with the largest

dx.doi.org/10.1021/jp304151e | J. Phys. Chem. B 2012, 116, 9467−9481

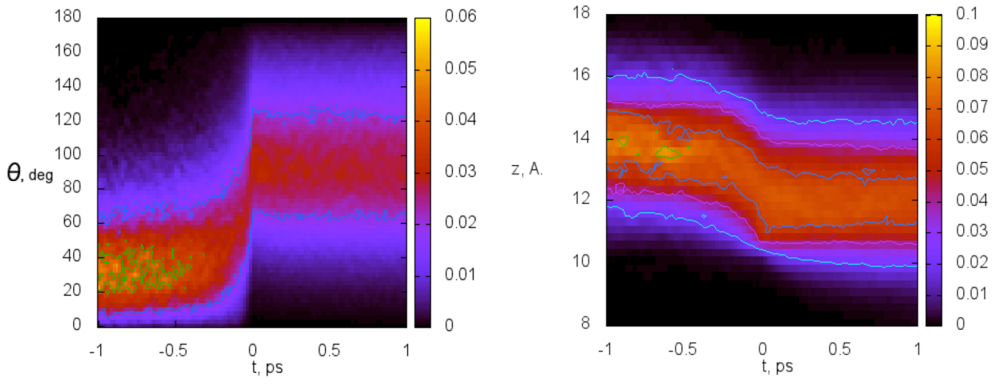

(a) (b)

Figure 11. Distribution of (a) θ and (b) z at each instant surrounding a free-to-bonded (HB2 criterion) transition described by interfacial OH groups of SPC/E water. $t = 0$ is defined as the instant at which the (previously free) OH groups first form hydrogen bonds. The distributions for $t < 0$ include only free OH groups; for $t > 0$ they include only bonded ones.

decay time also has the largest amplitude (and so τ_{ex} is the largest of the two decay times obtained in the fit), here both exponentials have comparable amplitudes (see Supporting Information for the fit parameters). For this reason the characteristic times $\tau_{f,b}$ and $\tau_{b,f}$ are given by the average of the two decay times obtained from the fit weighed by the amplitude of each exponential. Inspection of the decay times in Table 5

Table 5. Characteristic Time (ps) for Free-to-Bonded ($\tau_{f,b}$) and Bonded-to-Free ($\tau_{b,f}$) Transitions[a]

	location	SPC/E	TIP4P/2005
$\tau_{f,b}$	interface	0.81	0.73
	bulk	0.18	0.16
$\tau_{b,f}$	interface	0.55	0.61
	bulk	0.58	0.67

[a]HB1 criterion for the bonded state and HB2 criterion for the free state.

makes it apparent that $\tau_{f,b}$ at the interface (0.7−0.8 ps) is larger than but still comparable to the duration of the free-to-bonded event (0.3 ps) at the interface. This indicates that either the free and bonded states at the interface are separated by a free energy barrier or that the free state lies at the bottom of a purely downhill free energy landscape. Below we show the latter situation applies but the free energy difference between the two states is small, so free-to-bonded transitions are still largely diffusive. For comparison, note that the characteristic time between hydrogen-bond exchanges in the bulk (3−4 ps; see Table 4) is considerably larger than the duration of the actual hydrogen-bond exchange event (≈0.2 ps; see Supporting Information). This large difference in time scales indicates that hydrogen-bond exchange is predominantly an activated process, a consequence of the sizable free energy barrier ($4.5k_BT$ for SPC/E water[74]) associated with this process.

Comparison of the $\tau_{f,b}$ and $\tau_{b,f}$ values shown in Table 5 indicates that the bonded-to-free transition time is almost identical at the interface and the bulk, but the reverse transition time is about 4 times longer at the interface than in the bulk. The quasi-independence of $\tau_{b,f}$ on the position of the water slab indicates that even though bonded-to-free transitions at the interface involve rotation in θ and translation in z, they are barely affected by the effective potentials in θ and z shown in Figure 6. This apparently nonintuitive result is easily understood by looking at the average trajectories in Figure 11: for a bonded-to-free transition—i.e., going from positive to negative values of t—z changes little near $t = 0$ and θ changes mostly after (i.e., for $t < 0$) the breakage of the hydrogen bond, so the rate of bonded-to-free transitions must be principally influenced by the effective potential landscape in the O···O distance and O−H···O angle of the hydrogen-bonded state. As this landscape is similar at the interface and in the bulk (as inferred from the $P_{HB}(d,\varphi)$ distributions shown in the Supporting Information and discussed above), $\tau_{b,f}$ is similar for these two water populations.

Free Energy Difference Associated with Free-to-Bonded Transitions of Long-Lived, Free, Interfacial OH Groups Is Approximately $3k_BT$. As mentioned above, free-to-bonded transitions become significantly less frequent at the interface than in the bulk ($\tau_{f,b}$ is longer at the interface). We note also that $\tau_{f,b}$ is not constant throughout the interface, but instead is larger for OH groups in the outer interfacial layers. This dependence on interfacial position is clearly visible in Figure 12,

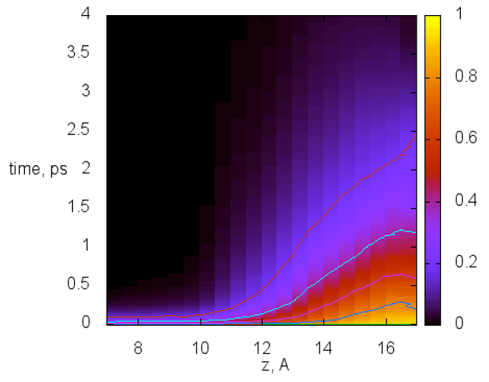

Figure 12. Values of $1 - C(\tau)$ (with $C(\tau)$ defined by eq 8) for free-to-bonded transitions, as a function of the position z of free SPC/E OH groups at $t = 0$.

which shows the $1 - C(\tau)$ function for free-to-bonded transitions as a function of the position z of the free OH groups at $t = 0$. The increase in $\tau_{f,b}$ for free OH groups in the outer interfacial regions is directly related to their average orientation in θ: as shown in Figure 5a, free OH groups in the outer interfacial regions are more upright, having both a narrower orientation distribution and lower average θ; in the

dx.doi.org/10.1021/jp304151e | J. Phys. Chem. B 2012, 116, 9467−9481

Supporting Information we show that more upright OH groups have longer lifetimes. The change in the free energy barrier, $\Delta\Delta G^{\ddagger}$, associated with free-to-bonded transitions of free OH groups in the outer interfacial region (i.e., those that are longer lived) relative to the bulk can be estimated by determining the $\tau_{f,b}$ for water molecules initially within a narrow, outer slice of the interface (e.g., for z = 15 Å in Figure 12), as $\tau_{f,b,z=15}/\tau_{f,b,bulk} = \exp(\Delta\Delta G^{\ddagger}/(k_BT))$: it is approximately $3k_BT$. To confirm that the increase in the rotational free energy barrier of free OH groups is associated with the free energy landscape in (θ,z) shown in Figure 6a, we calculate the maximum added energy cost of rotating a free OH group at z = 15 Å from the free energy minimum (θ = 0) to the position of the nearest free energy minimum for bonded OH groups ($\theta \approx >90°$ in Figure 6b) relative to the same rotation in the bulk. This added cost is also approximately $3k_BT$, suggesting that the free energy landscape in (θ,z) shown in Figure 6a should be the principal reason behind the lower free-to-bonded transition rates at the interface. As the characteristic time for free-to-bonded transitions in the bulk is very small (<200 fs, see Table 5), there is no significant energy barrier associated with these transitions in the bulk. This fact, together with the free energy landscape shown in Figure 6a, indicates that free-to-bonded transitions at the interface are, strictly speaking, barrierless; they are better described as a diffusive escape from a shallow ($3k_BT$) free energy well.

5. CONCLUDING REMARKS

At the air/water interface ≈75% of OH groups are known to be hydrogen-bonded and point toward the liquid while 25% are free and point toward the vapor. In our previous report we addressed, through both experiment and computation, the ultrafast reorientational dynamics of the free OH at time scales of ≤1 ps.[8] Here we report simulations that deepen our understanding of the dynamics of free OH groups for longer time scales and also address the larger, hydrogen-bonded OH population. We find that, in general, interfacial hydrogen-bonded OH groups rotate with very similar rates and via the same mechanism as bulk OH groups: for both populations, OH groups rotate via infrequent large-amplitude angular jumps between stable O−H···O complexes and, in between jumps, collective rotation of those complexes (i.e., frame rotation). While interfacial hydrogen-bonded OH groups rotate at the same rate as the bulk groups and through the same mechanism, they experience both faster frame rotation and smaller jump frequency: these two effects counteract each other. Both the enhanced frame rotation and the decreased jump frequency are the result of the decrease in time- and space-averaged density (relative to the bulk) at the air/water interface; i.e., they are a direct consequence of capillary waves. In contrast, interfacial free OH groups rotate both more quickly than bulk groups and diffusively.

Over the past several decades a variety of workers have demonstrated that the structure of water as measured by local water density fluctuations—whether they be in the bulk, near small solutes, near macromolecular solutes, or near extended surfaces—can be used to rationalize the thermodynamics of solvation and assembly.[80−90] While this insight is important, it is still fundamentally descriptive: given a solute of particular structure, one cannot predict how it will affect local water density fluctuations and therefore the thermodynamic properties of its solvation. Recent work by us and others suggests a way forward: we have previously shown that the rate of density change occurs (in bulk water and near disaccharides) on the same time scales over which hydrogen bonds break and reform.[74] Similarly, computational studies of protein folding in a variety of systems make clear that hydrophobic collapse occurs on time scales similar to those of bulk water structural change.[6,7,91,92] In a recent study of water near several proteins by Chandler, Garde, and co-workers,[93] local density fluctuations of water close to certain portions of the protein surface were found to obey a bimodal distribution with enhanced low density fluctuations. This enhancement was interpreted by the authors to suggest that interfacial water near these portions of the protein surface was near a dewetting phase transition. A number of prior studies have shown that waters at hydrophobic interfaces may have one OH group that points toward the adjoining phase and is, at best, weakly hydrogen-bonded, and one OH group that points toward the liquid and is strongly hydrogen-bonded to other waters.[59] In this study we illustrate that, for the air/water interface (a model hydrophobic interface), the interfacial perturbation of the structural dynamics of the hydrogen-bonded OH groups is modest. It therefore seems likely that density fluctuations that require rotating these types of OH groups will be similar to those in the bulk. In contrast, for free OH groups the interfacial perturbation is large: they rotate both substantially more rapidly and through a different mechanism than bulk groups. It therefore seems likely that the sort of density fluctuations required for dewetting transitions at protein surfaces require protein topology that strongly enhances the local population of free OH groups.

■ ASSOCIATED CONTENT

Ⓢ Supporting Information

NAMD-compatible parameter and topology files for TIP4P/2005 water, fraction of water molecules with one or two free OH groups at each position in the water slab, residence time of waters at the interface, $P(\theta)$ for the three hydrogen-bond criteria, comparison of the orientation of OH groups at the air/water interface and at the air/hydrophobic interface,[23] $P(\theta)$ of free OH groups as a function of their lifetime, lifetime of free OH groups as a function of their orientation in θ at t = 0, two-dimensional histograms characterizing the hydrogen-bonded state in terms of the O−H···O angle and the O···O distance, lifetimes of the free and hydrogen-bonded states, cartoon of the hydrogen-bond exchange mechanism, distance and angle trajectories associated with hydrogen-bond exchange, frame decay, mean square displacement plot, and calculation of mean square angular displacement, fitting parameters for free-to-bonded and bonded-to-free transitions. This material is available free of charge via the Internet at http://pubs.acs.org.

■ AUTHOR INFORMATION

Corresponding Author

*E-mail: ana.vilaverde@mpikg.mpg.de (A.V.V.); p.g.bolhuis@uva.nl (P.G.B.); campen@fhi-berlin.mpg.de (R.K.C.).

Present Address

[§]Theory and Bio-Systems Department, Max Planck Institute of Colloids and Interfaces, Wissenschaftspark Potsdam-Golm, Am Mühlenberg 1 OT Golm, 14476 Potsdam, Germany. Also at Physics Center, University of Minho, Campus de Gualtar, 4710-057 Braga, Portugal.

Notes

The authors declare no competing financial interest.

■ ACKNOWLEDGMENTS

A.V.V. thanks Dr. Peter Freddolino for help using the TIP4P/2005 model in NAMD, and Dr. Nils Becker for useful discussions. This work is part of the research program of the Stichting Fundamenteel Onderzoek der Materie with financial support from the Nederlanse Organisatie voor Wetenschappelijk Onderzoek. We thank SARA Computing and Networking Services (www.sara.nl) for their support in using the Lisa Compute Cluster.

■ REFERENCES

(1) Brown, G.; Henrich, V.; Casey, W.; Clark, D.; Eggleston, C.; Felmy, A.; Goodman, D.; Gratzel, M.; Maciel, G.; McCarthy, M.; Nealson, K.; Sverjensky, D.; Toney, M.; Zachara, J. *Chem. Rev.* **1999**, *99*, 77−174.
(2) Sverjensky, D. *Geochim. Cosmochim. Acta* **2005**, *69*, 225−257.
(3) Rønne, C.; Astrand, P.; Keiding, S. *Phys. Rev. Lett.* **1999**, *82*, 2888−2891.
(4) Rønne, C.; Keiding, S. R. *J. Mol. Liq.* **2002**, *101*, 199−218.
(5) Qvist, J.; Halle, B. *J. Am. Chem. Soc.* **2008**, *130*, 10345−10353.
(6) Bakker, H. J. *Chem. Rev.* **2008**, *108*, 1456−1473.
(7) Bakker, H. J.; Skinner, J. L. *Chem. Rev.* **2010**, *110*, 1498−1517.
(8) Hsieh, C.-S.; Campen, R. K.; Verde, A. C. V.; Bolhuis, P.; Nienhuys, H.-K.; Bonn, M. *Phys. Rev. Lett.* **2011**, *107*, 116102.
(9) Kuo, I.; Mundy, C. *Science* **2004**, *303*, 658−660.
(10) Kühne, T. D.; Pascal, T. A.; Kaxiras, E.; Jung, Y. *J. Phys. Chem. Lett.* **2011**, *2*, 105−113.
(11) Hantal, G.; Darvas, M.; Partay, L. B.; Horvai, G.; Jedlovszky, P. *J. Phys.: Condens. Matter* **2010**, *22*, 284112.
(12) Andreae, M. O.; Crutzen, P. J. *Science* **1997**, *276*, 1052−1058.
(13) Du, Q.; Superfine, R.; Freysz, E.; Shen, Y. R. *Phys. Rev. Lett.* **1993**, *70*, 2313−2316.
(14) Du, Q.; Freysz, E.; Shen, Y. *Science* **1994**, *264*, 826−828.
(15) Richmond, G. *Chem. Rev.* **2002**, *102*, 2693−2724.
(16) Gan, W.; Wu, D.; Zhang, Z.; Ran Feng, R.; Wang, H.-F. *J. Chem. Phys.* **2006**, *124*, 114705.
(17) Fan, Y.; Chen, X.; Yang, L.; Cremer, P. S.; Gao, Y. Q. *J. Phys. Chem. B* **2009**, *113*, 11672−11679.
(18) Taylor, R. S.; Dang, L. X.; Garrett, B. C. *J. Phys. Chem.* **1996**, *100*, 11720−11725.
(19) Kuo, I. F. W.; Mundy, C. J.; McGrath, M. J.; Siepmann, J. I. *J. Chem. Theory Comput.* **2006**, *2*, 1274−1281.
(20) Baer, M. D.; Mundy, C. J.; McGrath, M. J.; Kuo, I. F. W.; Siepmann, J. I.; Tobias, D. J. *J. Chem. Phys.* **2011**, *135*, 124712.
(21) Laage, D.; Hynes, J. T. *J. Phys. Chem. B* **2008**, *112*, 14230−14242.
(22) Laage, D.; Stirnemann, G.; Sterpone, F.; Rey, R.; Hynes, J. T. *Annu. Rev. Phys. Chem.* **2011**, *62*, 395−416.
(23) Stirnemann, G.; Sterpone, F.; Laage, D. *J. Phys. Chem. B* **2011**, *115*, 3254−3262.
(24) Stirnemann, G.; Castrillón, S. R.-V.; Hynes, J. T.; Rossky, P. J.; Debenedetti, P. G.; Laage, D. *Phys. Chem. Chem. Phys.* **2011**, *13*, 19911−19917.
(25) Berendsen, H. J. C.; Grigera, J. R.; Straatsma, T. P. *J. Phys. Chem.* **1987**, *91*, 6269−6271.
(26) Jorgensen, W. L.; Chandrasekhar, J.; Madura, J. D.; Impey, R. W.; Klein, M. L. *J. Chem. Phys.* **1983**, *79*, 926−935.
(27) Abascal, J. L. F.; Vega, C. *J. Chem. Phys.* **2005**, *123*, 234505.
(28) Alejandre, J.; Chapela, G. A. *J. Chem. Phys.* **2010**, *132*, 014701.
(29) Phillips, J. C.; Braun, R.; Wang, W.; Gumbart, J.; Tajkhorshid, E.; Villa, E.; Chipot, C.; Skeel, R. D.; Kale, L.; Schulten, K. *Comput. Chem.* **2005**, *26*, 1781−1802.
(30) Humphrey, W.; Dalke, A.; Schulten, K. *J. Mol. Graphics* **1996**, *14*, 33−38.
(31) Smit, B. *J. Chem. Phys.* **1992**, *96*, 8639−8640.
(32) Ismail, A. E.; Grest, G. S.; Stevens, M. J. *J. Chem. Phys.* **2006**, *125*, 014702.
(33) Janeček, J. *J. Phys. Chem. B* **2006**, *110*, 6264−6269.
(34) Alejandre, J.; Tildesley, D. J.; Chapela, G. A. *J. Chem. Phys.* **1995**, *102*, 4574−4583.
(35) Trokhymchuk, A.; Alejandre, J. *J. Chem. Phys.* **1999**, *111*, 8510−8523.
(36) Wood, W. W. In *Physics of Simple Liquids*; Temperley, H. N. V., Rowlinson, J. S., Rushbrooke, G. S., Eds.; North-Holland: Amsterdam, 1968; Chapter 5, pp 151−155.
(37) Chitra, R.; Yashonath, S. *J. Phys. Chem. B* **1997**, *101*, 5437−5445.
(38) *CRC Handbook of Chemistry and Physics*; Haynes, W. M., Lide, D. R., Eds.; CRC Press: Boca Raton, FL, USA, 2011.
(39) Kuo, I.-F. W.; Mundy, C. J.; Eggimann, B. L.; McGrath, M. J.; Siepmann, J. I.; Chen, B.; Vieceli, J.; Tobias, D. J. *J. Phys. Chem. B* **2006**, *110*, 3738−3746.
(40) Pojjak, K.; Darvas, M.; Horvai, G.; Jedlovszky, P. *J. Phys. Chem. C* **2010**, *114*, 12207−12220.
(41) Kathmann, S. M.; Kuo, I.-F. W.; Mundy, C. J.; Schenter, G. K. *J. Phys. Chem. B* **2011**, *115*, 4369−4377.
(42) Benjamin, I. *Phys. Rev. Lett.* **1994**, *73*, 2083−2086.
(43) Sokahn, B. V. P.; Tildesley, D. J. *Mol. Phys.* **1997**, *92*, 625−640.
(44) Morita, A.; Hynes, J. T. *Chem. Phys.* **2000**, *258*, 371−390.
(45) Morita, A.; Hynes, J. T. *J. Phys. Chem. B* **2001**, *106*, 673−685.
(46) Perry, A.; Neipert, C.; Kasprzyk, C. R.; Green, T.; Space, B.; Moore, P. B. *J. Chem. Phys.* **2005**, *123*, 144705-11.
(47) Petersen, P. B.; Saykally, R. J. *Annu. Rev. Phys. Chem.* **2006**, *57*, 333−364.
(48) Evans, R. *Adv. Phys.* **1979**, *28*, 143−200.
(49) Sedlmeier, F.; Horinek, D.; Netz, R. R. *Phys. Rev. Lett.* **2009**, *103*, 136102.
(50) Chacón, E.; Tarazona, P.; Alejandre, J. *J. Chem. Phys.* **2006**, *125*, 014709.
(51) Jorge, M.; Jedlovszky, P.; Cordeiro, M. N. D. S. *J. Phys. Chem. C* **2010**, *114*, 11169−11179.
(52) Willard, A. P.; Chandler, D. *J. Phys. Chem. B* **2010**, *114*, 1954−1958.
(53) Liu, W.-T.; Zhang, L.; Shen, Y. R. *J. Chem. Phys.* **2006**, *125*, 144711.
(54) Byrnes, S. J.; Geissler, P. L.; Shen, Y. R. *Chem. Phys. Lett.* **2011**, *516*, 115−124.
(55) Cappa, C. D.; Smith, J. D.; Wilson, K. R.; Saykally, R. J. *J. Phys.: Condens. Matter* **2008**, *20*, 205105.
(56) Varilly, P. S. Fluctuations in Water and Their Relation to the Hydrophobic Effect. Ph.D. Thesis, University of California, Berkeley, 2011.
(57) Tuckerman, M. E. *Statistical Mechanics: Theory and Molecular Simulation*; Oxford University Press: Oxford, U.K.2011.
(58) Goh, M. C.; Hicks, J. M.; Kemnitz, K.; Pinto, G. R.; Heinz, T. F.; Eisenthal, K. B.; Bhattacharyya, K. *J. Phys. Chem.* **1988**, *92*, 5074−5075.
(59) Stirnemann, G.; Rossky, P. J.; Hynes, J. T.; Laage, D. *Faraday Discuss.* **2010**, *146*, 263−281.
(60) Jedlovszky, P. *J. Phys.: Condens. Matter* **2004**, *16*, S5389−S5402.
(61) Laage, D.; Hynes, J. T. *Chem. Phys. Lett.* **2006**, *433*, 80−85.
(62) Scott, J. N.; Vanderkooi, J. M. *Water* **2010**, *2*, 14−28.
(63) Wilson, K. R.; Schaller, R. D.; Co, D. T.; Saykally, R. J.; Rude, B. S.; Catalano, T.; Bozek, J. D. *J. Chem. Phys.* **2002**, *117*, 7738−7744.
(64) This function has the advantage of being directly measurable from pump−probe spectroscopy for water in the bulk, allowing for direct comparison between experiment and simulation in these systems.[65] The structural dynamics of interfacial OH groups, as sampled in polarization resolved IR pump/VSF probe experiment, sample substantially more complicated correlation functions.[66]
(65) Lin, Y. S.; Pieniazek, P. A.; Yang, M.; Skinner, J. L. *J. Chem. Phys.* **2010**, *132*, 174505.
(66) Gengeliczki, Z.; Rosenfeld, D. E.; Fayer, M. D. *J. Chem. Phys.* **2010**, *132*, 244703.
(67) Ludwig, R.; Weinhold, F.; Farrar, T. C. *J. Chem. Phys.* **1995**, *103*, 6941−6950.

(68) Bakker, H. J.; Rezus, Y. L. A.; Timmer, R. L. A. *J. Phys. Chem. A* **2008**, *112*, 11523−11534.
(69) Laage, D.; Hynes, J. T. *Science* **2006**, *311*, 832−835.
(70) Northrup, S. H.; Hynes, J. T. *J. Chem. Phys.* **1980**, *73*, 2700−2714.
(71) Laage, D.; Stirnemann, G.; Hynes, J. T. *J. Phys. Chem. B* **2009**, *113*, 2428−2435.
(72) Ivanov, E. N. *Sov. Phys. JETP* **1964**, *18*, 1041−1045.
(73) In the derivation of eq 7 jumps are assumed to be spatially isotropic. This is clearly not the case at an interface. In this environment, jumps in the *XY* plane remain isotropic but jumps in θ are not. However, Figure 4a shows that the $P(\theta)$ distribution for the hydrogen-bonded OH groups has a maximum value near 90° and low skewness—similar to the sine function that characterizes an isotropic distribution—indicating that approximating the jump probability as isotropic should not introduce significant error.
(74) Vila Verde, A.; Campen, R. K. *J. Phys. Chem. B* **2011**, *115*, 7069−7084.
(75) Mazza, M. G.; Giovambattista, N.; Starr, F. W.; Stanley, H. E. *Phys. Rev. Lett.* **2006**, *96*, 057803.
(76) Mazza, M. G.; Giovambattista, N.; Stanley, H. E.; Starr, F. W. *Phys. Rev. E* **2007**, *76*, 031203.
(77) Note that ϕ and θ are the azimuthal and polar angles of a spherical coordinate system, but ω is simply the angular distance between any two points at the surface of a sphere.
(78) Berg, H. C. *Random Walks in Biology*; Princeton University Press: Princeton, NJ, USA, 1993.
(79) Metzler, R.; Klafter, J. *Phys. Rep.* **2000**, *339*, 1−77.
(80) Garde, S.; Hummer, G.; Garcia, A.; Paulaitis, M.; Pratt, L. *Phys. Rev. Lett.* **1996**, *77*, 4966−4968.
(81) Hummer, G.; Garde, S.; Garcia, A.; Pohorille, A.; Pratt, L. *Proc. Natl. Acad. Sci. U.S.A.* **1996**, *93*, 8951−8955.
(82) Hummer, G.; Garde, S. *Phys. Rev. Lett.* **1998**, *80*, 4193−4196.
(83) Lum, K.; Chandler, D.; Weeks, J. *J. Phys. Chem. B* **1999**, *103*, 4570−4577.
(84) Huang, D.; Chandler, D. *Proc. Natl. Acad. Sci. U.S.A.* **2000**, *97*, 8324−8327.
(85) Siebert, X.; Hummer, G. *Biochemistry* **2002**, *41*, 2956−2961.
(86) Chandler, D. *Nature* **2005**, *437*, 640−647.
(87) Athawale, M. V.; Jamadagni, S. N.; Garde, S. *J. Chem. Phys.* **2009**, *131*, 115102.
(88) Acharya, H.; Vembanur, S.; Jamadagni, S. N.; Garde, S. *Faraday Discuss.* **2010**, *146*, 353−365.
(89) Patel, A. J.; Varilly, P.; Chandler, D. *J. Phys. Chem. B* **2010**, *114*, 1632−1637.
(90) Patel, A. J.; Varilly, P.; Jamadagni, S. N.; Acharya, H.; Garde, S.; Chandler, D. *Proc. Natl. Acad. Sci. U.S.A.* **2011**, *108*, 17678−17683.
(91) Zhou, R.; Huang, X.; Margulis, C.; Berne, B. *Science* **2004**, *305*, 1605−1609.
(92) Liu, P.; Huang, X.; Zhou, R.; Berne, B. *Nature* **2005**, *437*, 159−162.
(93) Patel, A. J.; Varilly, P.; Jamadagni, S. N.; Hagan, M. F.; Chandler, D.; Garde, S. *J. Phys. Chem. B* **2012**, *116*, 2498−2503.